Impedance Model Domains for the Stability Analysis of Multi-Inverter-Based-Resources Systems

Keijo Jacobs[1], Renan Morais Furlaneto[1], Dabeaurard Tho[1], Nasim Rashidirad[2], Jean Mahseredjian[1], and Antoine Lesage-Landry[1]

[1] *Dpt. of Electrical Engineering*
Polytechnique Montreal
Montreal, Canada
keijo.jacobs@polymtl.ca

[2] *Dpt. of Simulation of Networks*
Hydro Quebec Research Institute
Varennes, Canada

***Abstract*—Modern power systems are increasingly dominated by inverter-based resources (IBRs), which rely on fast control systems for its power-electric converters. These IBRs are vulnerable to oscillating interactions with other grid components. The stability of such power systems can be studied through impedance-based stability assessment. Different impedance modelling domains offer varying trade-offs in terms of accuracy, ease of implementation, and interpretability. Each provides distinct insight into the dynamic behavior and control interactions of the system. This paper presents a concise comparative overview of impedance model types, illustrating their practical implications through representative case studies. All impedance models are measured from detailed electromagnetic transient models.**

Keywords*—*impedance-based stability assessment, impedance scanning, inverter-based resources, impedance model domain

I. Introduction

With the global shift toward renewable energy integration, power systems are increasingly populated by converter-interfaced generation. These converters exhibit fast control dynamics, introducing a heightened risk of oscillatory instabilities. Such phenomena are classified as resonance stability or converter-driven stability [1]. Real-world incidents, including large-scale outages and equipment damage, have underscored the urgency of conducting detailed stability assessment tailored to inverter-based resources (IBRs) and their interaction with the grid [2].

Impedance-based stability assessment (IBSA) is a widely used technique for evaluating the dynamic interactions in power systems. The method typically involves partitioning the system into two subsystems, such as the grid and the converter, whose small-signal impedances form a feedback loop equivalent. Stability can then be assessed by analyzing the loop gain using Bode plots, Nyquist plots, or *RX* diagrams, which reveal potential resonance or control-induced instabilities [3]. While impedance models can be derived analytically from detailed system equations, this approach is often impractical for grid operators who lack access to proprietary control structures of commercial IBRs. In such cases, impedance scanning, i.e. perturbation and response measurements, offers a practical alternative for extracting impedance characteristics.

Many grid components, such as transformers, cables, and passive filters, can be adequately represented using single-input single-output (SISO) impedance models in the sequence domain. However, it is well established that certain technologies require multi-input multi-output (MIMO) impedances to capture their full behavior (Table II in [1]). A key indicator of this behavior is the presence of asymmetry in the off-diagonal elements of the MIMO impedance [4]. This asymmetry causes the mirror-frequency effect [5], where a single oscillatory mode manifests at two frequencies (oscillatory frequency and mirror frequency) symmetrically located around the fundamental. Accurate modeling of this effect is essential for assessing resonance and control interactions in converter-dominated grids.

This paper presents a concise summary of impedance model domains for assessing mirror-frequency coupling and the stability of multi-IBR systems, i.e. power systems with more than one, and potentially different types of IBRs. It aims to illustrate characteristics and differences of the modelling domains, providing an intuitive understanding, while referencing mathematical detail for further reading. Impedance scanning for the different domains and the conversions between them are described and compared, serving as a guide for using these techniques during visual assessment of system characteristics. Detailed and generic electro-magnetic transient (EMT) models of four distinct grid components are the source for the scanned impedance models.

Section II provides a summary of the scanning and domain conversion methods. Section III shows the impedances of four case studies. Section IV concludes the paper and provides practical guidelines.

II. Impedance Modelling Principles

A. Impedance Modelling Domains

From [6] and [7] it has been concluded that positive sequence domain (p, SISO), rotating [5] and stationary [7] coupled sequence domain (rcs and scs, 2×2 MIMO), and the dq domain (dq, 2×2 MIMO) are generally useful for the analysis of IBRs' impedance characteristics, whereas other domains may be useful in specific cases. Different impedance model domains offer distinct trade-offs in terms of clarity for visual assessment, implementation complexity, accuracy, and suitability for IBSA. The *p-impedance model* is visually and mathematically straightforward and requires only a single measurement per data point. However, it cannot capture coupling phenomena such as

979-8-3315-8138-1

mirror frequency coupling (MFC). The *dq-impedance model,* rotating with the fundamental frequency, f_1, captures coupling effects between d- and q-axes but is less intuitive for power system stability studies, since couplings are not visually assessable [8]. Scanning requires two linearly independent perturbations and measurements at each f_{dq}. The *rcs-impedance model* offers visual assessment of coupling via the off-diagonal impedance matrix elements, but scanning is more complex due to the need to reference perturbations and measurements at two distinct frequencies, f_p and f_n, with additional distinctions for f_n (section II.C). This impedance model is very similar to the modified sequence domain presented in [5], but uses the dq-frequency as reference frame. The *scs-impedance model* allows for coupling assessment directly in the positive sequence frequency, which aligns better with conventional power system engineering intuition.

B. Impedance Scanning

For IBSA the system needs to be split into two subsystems. Each subsystem is scanned and the resulting impedances can be used for assessment via Bode- or Nyquist plots. A simplified schematic for the scanning procedure is shown in Fig. 1, where * represents the impedance domain, f_{pert} and A_{pert} the perturbation frequency and amplitude, v_m and i_m the measured voltage and current, and T_{DFT} the discrete Fourier transform (DFT) window. The presented implementation enables to halt the simulation upon reaching a steady-state response to the perturbation. This allows for significant computational savings compared to fixed simulation time and post-simulation processing. Note that f_1 is only required for the transforms for dq-scanning and the axis 2 is not required for p-scanning.

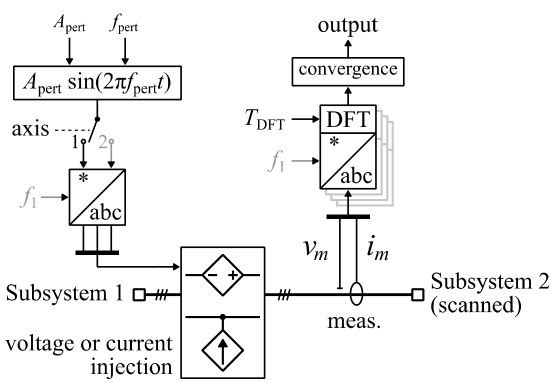

Fig. 1. Simplified view of frequency scanning procedure with * representing the scanning domain; relevant variables are listed in Table I.

The main differences for scanning in different impedance domains, as summarized in Table I, are

1. the number of required perturbations and measurements;
2. the number of required signal transforms between the impedance domain and the abc-domain of the power system EMT model, and the DFTs;
3. perturbation and measurement frequencies;
4. the need for computing the MIMO impedances post-simulation, when two simulation runs are required.

Table I. Differences for scanning parameters, signal processing, and output for p-, dq-, and rcs-scanning

Type	Axis	f_{pert}	Transform & DFT	Output
Scan run 1				
p	1	f_p	$2\times f_p$	Z_p
dq	1 (d)	f_{dq}	$2\times f_{dq}$	$I_{dd}, I_{qd}, V_{dd}, V_{qd}$
rcs	1 (p)	f_p	$2\times f_p$ $2\times f_n$	$I_{pp}, I_{np}, V_{pp}, V_{np}$
Scan run 2				
p	No second run required			
dq	2 (q)	f_{dq}	$2\times f_{dq}$	$I_{dq}, I_{qq}, V_{dq}, V_{qq}$
rcs	2 (n)	f_n	$2\times f_p$ $2\times f_n$	$I_{pn}, I_{nn}, V_{pn}, V_{nn}$

To the best of the authors' knowledge, the dq-scan consistently converges earlier than the rcs-scan, resulting in a faster computation time. The p-scan is the computationally fastest method [6]. The scs-scan is not used in this work since the result is equal to the rcs-scan. For further detail, see [7].

C. Model Conversion

The impedance models can be converted between the domains, as shown in Fig. 2, and detailed in [6]. For the purpose of the investigations shown in this paper it is important to note that there is no information loss when converting between dq-, rcs-, and scs-impedances. Scanning in these MIMO-frames yields the same results. Therefore, most of the plots only show one MIMO scan for better clarity of the plots. However, due to signal processing, convergence criteria, and reference frequency synchronization there might be negligible discrepancies or artefacts between the scans in these domains. The MIMO impedance models are denoted by the bold symbol **Z**, whereas the SISO model is denoted by *Z*.

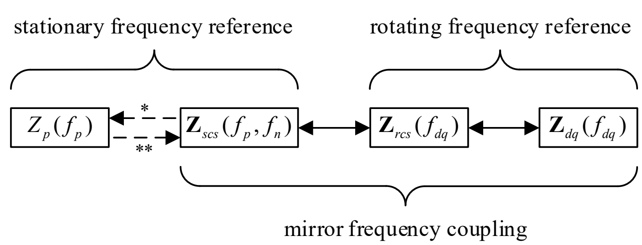

Fig. 2. Conversions between impedance domains.
* non-reversible simplification, ** assuming zero off-diagonal elements.

The conversion operations between the model domains are listed in Table II. The dq-impedance can be converted to the rcs-impedance through the transformation matrix **C**. The frequency shift described for the modified sequence, in [5], is not performed so that the rcs-model refers to the synchronously rotating frequency reference. This has the advantage over the dq-model that symmetric inductive behavior is eliminated from the-off-diagonal elements so that cross-axis coupling becomes isolated and visible (e.g. an *RL* circuit will exhibit off-diagonal elements in dq- but not in rcs-domain). The rcs-impedance can be converted into scs-domain by applying the frequency shift described in [5]. Additional operations are needed to obtain the subsynchronous region, i.e. impedances for negative sequence

979-8-3315-8138-1

frequencies with negative sign become impedances for positive sequence with positive sign. For the MIMO models the matrix elements are individually conjugated and then rotated by 180°.

A conversion from scs- to p-impedance simplifies the model by combining the off-diagonal matrix elements with the diagonal ones. Asymmetric coupling as exhibited by grid components with the mirror-frequency effect will lead to a different p-model as compared to an impedance obtained from a p-scan. However, components that exhibit symmetric coupling through the off-diagonal elements of the MIMO models will yield the same result as the p-scan. This operation is not reversible as it entails information loss, but for mirror-frequency decoupled systems, e.g. constant parameter transmission lines, the p-impedance can be converted to scs-impedance by assuming the negative sequence symmetrical to the positive sequence, and setting the off-diagonal elements to zero.

Table II. Conversion between impedance domains

	Operation
$\mathbf{Z}_{dq}$ ⇕ $\mathbf{Z}_{rcs}$	Transformation matrix $\mathbf{Z}_{rcs}\left(f_{dq}\right)=\mathbf{C}\mathbf{Z}_{dq}\left(f_{dq}\right)\mathbf{C}^{-1}$, with $\mathbf{C}=\frac{1}{\sqrt{2}}\begin{bmatrix}1 & j\\ 1 & -j\end{bmatrix}$
$\mathbf{Z}_{rcs}$ ⇕ $\mathbf{Z}_{scs}$	Frequency shift for $f \geq f_1$: $\mathbf{Z}_{scs}\left(f_p=f_{dq}+f_1\right)=\mathbf{Z}_{rcs}\left(f_{dq}\right)$ Frequency shift, conjugate, and matrix rotation for $0 \leq f < f_1$: $\mathbf{Z}_{scs}\left(f_n\right)=\begin{bmatrix}Z^*_{rcs,nn}\left(f_n\right) & Z^*_{rcs,np}\left(f_n\right)\\ Z^*_{rcs,pn}\left(f_n\right) & Z^*_{rcs,pp}\left(f_n\right)\end{bmatrix}$, $f_n=\left\|f_{dq}-f_1\right\|$
$\mathbf{Z}_{scs}$ ⇓ Z_p	Simplification $Z_p\left(f_p\right)=\dfrac{\det\left(\mathbf{Z}_{scs}\left(f_p\right)\right)}{Z_{nn}\left(f_p\right)}$
Z_p ⇓ $\mathbf{Z}_{scs}$	Assume no coupling $\mathbf{Z}_{scs}\left(f_p\right)=\begin{bmatrix}Z_p\left(f_p\right) & 0\\ 0 & Z_n\left(f_n\right)\end{bmatrix}$

III. Case Studies and Observations

The scanned EMT models feature complex control systems and dynamics and, due to the page limitations, the parameters and diagrams can not be shown here. For full detail, readers may consult the referenced material. Impedance models are obtained and visualized for four case studies:

1. a passive grid section model of a single-IBR system;
2. a doubly-fed induction generator (DFIG) wind park (WP) of a single-IBR system, with a small range of MFC around fundamental;
3. a MFC full-scale converter (FSC) WP in a single-IBR system with a large range of MFC in the supersynchronous region;
4. a grid-forming (GFM) converter in a multi-IBR system with MFC in a small frequency range around fundamental.

The legend in each figure denotes the domain of the model with the scan type in parentheses. For example, “p (rcs-scan)” denotes an impedance which has been scanned in rcs-domain and then converted into a p-impedance. All figure axis labels are general notations that should be understood in the domain of the plotted impedance model. Different domains are present in the same plot, so that, e.g., R_{11} and f refer to (1) resistance of the dd-element and the dq-frequency for a dq-impedance; (2) resistance of the pp-element and positive sequence frequency for an scs-impedance; (3) the resistance of the SISO impedance and positive sequence frequency for a p-impedance.

A. Passive Grid Section

Fig. 3 shows the MIMO impedance characteristics obtained from scanning a grid section featuring constant parameter lines and equivalent impedances, i.e., a passive, linear, and non-coupled subsystem, as in Fig. 6 of [6]. Scans in p-, rcs-, and dq-domain are compared in scs-domain. Note that the p-scan can not capture the off-diagonal elements, so they are set to zero during the conversion to scs-impedance. The *first observation* is that the dq-impedance exhibits non-zero values in the off-diagonal elements. Hence, it is less intuitive for the visual inspection of mirror frequency coupling. This is because reactive characteristics of the scanned system manifest in the real-part of the off-diagonal elements [5]. The characteristic seen in the off-diagonal elements is, therefore, not indicative of mirror-frequency coupling. Throughout the rest of the paper, the dq-impedance is not depicted for better clarity of the plots and the brevity of the paper. The conversion of the dq-impedance to scs-domain yields a matching result, illustrating equivalence. The *second observation* is that the off-diagonal elements of the scs-impedance are zero, which simplifies the visual assessment of coupling compared to the dq-form. The *third observation* is that the characteristic of the scs-form close to 0 Hz in the 11-element is observable mirrored around the 120 Hz line in the 22-element, which perfectly illustrates the frequency shift and the presence of two reference frequencies in the scs-domain, as shown in Table II. Note that the negative sequence impedance is not explicitly provided. Because positive and negative sequence are symmetric, the impedance characteristic in the 11-element can be mirrored into the negative frequency range, which manifests in the symmetry of the 22-element around 120 Hz.

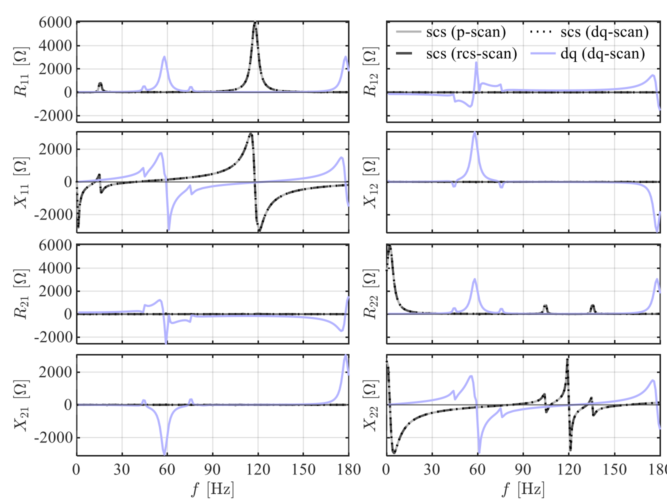

Fig. 3. MIMO RX-plot of a passive grid section.

979-8-3315-8138-1

B. DFIG Wind Park

The DFIG WP example is presented in Fig. 6 of [6]. Upon inspection of the rcs-scan results in scs-domain, depicted as a magnitude-angle plot in Fig. 4, significant non-zero values can be observed in the off-diagonal elements between 40 and 80 Hz. The *first observation* is that the 12- and the 21-element are significant but mostly symmetric, as indicated by the change in sign for the angle. Quantitative measures for coupling assessment are presented in [1]. For the analysis in this limited scope it suffices to compare the difference between rcs-scan and p-scan in scs-domain. The off-diagonal elements for the p-scan are assumed zero for the conversion to scs-domain. The *second observation* is that p-scan and rcs-scan show clear differences between 45 and 75 Hz, which demonstrates the error caused by neglecting coupling effects of the DFIG control.

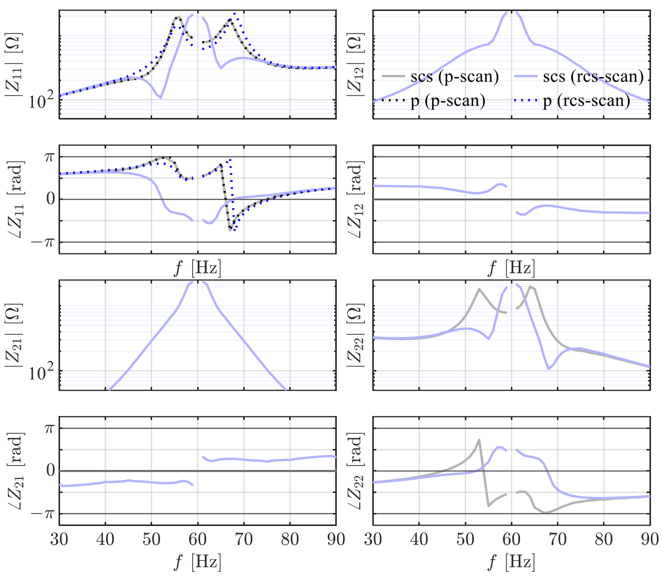

Fig. 4. MIMO magnitude ands angle plot of the DFIG WP impedance.

The *third observation* is that the models become identical below 40 and above 80 Hz (full range not shown here to improve the visibility of model inaccuracies). This supports the findings in [6], where a negatively damped mode at 26 Hz shows a negligibly small, but non-zero mirror frequency component at 94 Hz. The p-scan and subsequent IBSA in p-domain is sufficiently accurate (in that specific frequency range) for the identification of the instability. This is also supported by looking at the p-impedance superposed in the 11-element of Fig. 4. However, it should be clear from these results that this is a specific and unique case, and the identification of the instability here does by no means imply that p-models are universally accurate. The authors would expect discrepancies between IBSA using the p- and the rcs-scan if the mode were to occur at 52 Hz, for example. The *fourth observation* is that, although asymmetric off-diagonal elements are present in the scs-impedance, their impact on p-impedance remains quite limited.

C. FSC Wind Park

The DFIG WP from the previous example is replaced by an FSC WP. Two configurations are scanned, where WP 1 has equal PI-controller parameters for the inner current control of d- and q- signals, and WP 2 has asymmetrical parameters, manifesting in asymmetrical coupling. Fig. 5 shows the impact on the p-impedance when using p-scan vs. rcs-scan. The *first observation* is that both WP models show differences for the entire frequency range, which suggests that inaccuracies in the stability analysis can be expected when using the p-scan. The *second observation* is that the p-impedance of WP 2 exhibits significant differences in the super-synchronous frequency range. For IBSA, this might manifest in different phase margin or gain crossover location for a Bode-plot assessment, for example, potentially leading to erroneous stability predictions.

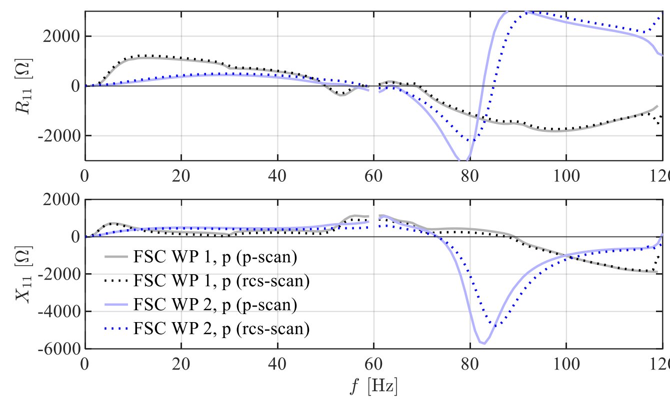

Fig. 5. SISO p-impedances from p-scan and rcs-scan for FSC WP 1 and 2.

D. Grid-Forming Converter in Multi-IBR System

The example system is slightly modified from [9]. One grid-forming (GFM) converter, one grid-following (GFL) converter, a constant PQ-load, and a grid equivalent with an ideal voltage source, are connected to a bus via Π-lines. When disconnecting the grid, the system becomes islanded and the GFM converter provides the voltage reference for the system. The simple dq-scan used for this work is not able to effectively synchronize to the fundamental in the islanded case. To circumvent the issue the rcs-scan is used [11].

Fig. 6 shows the scs- and p-impedances for the GFM converter in magnitude-angle format. The *first observation* from the scs-impedance is that coupling is asymmetric as indicated by the different angle of the off-diagonal elements. The *second observation* is that the p-impedance angle for the rcs-scan flips sign at 56 Hz, which can be attributed to a badly chosen droop control coefficient. This is not captured by the p-scan which is superposed in the 11-element. In contrast to the case described in section III.B, where an interaction is located in the accurate frequency range of the p-impedance [6], an interaction between the GFM and a strong system is possible within the inaccurate range of the p-impedance for this case [10]. Indeed, the simulation exhibits an oscillation at 55 Hz with a mirror-frequency component of lower amplitude at 65 Hz, which can be observed from IBSA or from the time-domain waveforms (not shown here). The *third observation* is that the 11-element of the scs-impedance (rcs-scan) is much closer to the p-scan than the p-impedance converted from the rcs-scan. This shows that for systems with significantly asymmetrical off-diagonal elements, the 11-element of the scs-impedance should not be analyzed as if it were a p-impedance. Similarities of the 11-element to the p-impedance can be misleading.

IBSA is performed to illustrate that erroneous stability predictions may result from using p-scanned models. Fig. 7 presents the Nyquist plot of the open-loop gain of the system at the GFM converter POI, $L = Z_{grid} Z_{GFM}^{-1}$. The Nyquist plot obtained from the MIMO-models encircles the -1 point confirming instability, according to the generalized Nyquist criterion. As described in [7], the eigenloci of positive and negative sequence overlap for the scs-model and the crossover of the positive sequence eigenlocus with the unit circle indicates an oscillation frequency of $f_p = 55.1$ Hz and a mirror-frequency of $f_n = 64.9$ Hz . The Nyquist plots from both dq- and rcs-models indicate $f_{dq} = -4.9$ Hz . The Nyquist plot obtained from the p-scans does not reveal instability. However, a gain margin of 1.5 dB at 56 Hz indicates a weakly damped mode. It should be noted that the grid impedance includes a GFL converter with asymmetric coupling. Therefore, the grid p-scan introduces additional error via Z_{grid} , as described in [5].

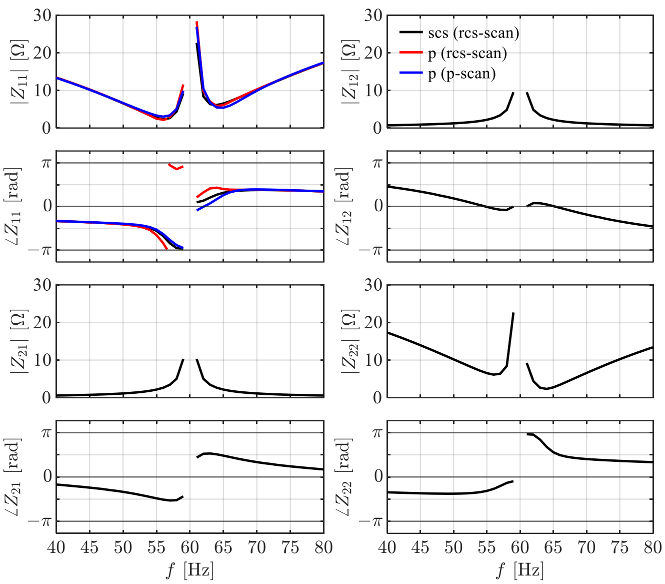

Fig. 6. MIMO magnitude and angle plot of GFM converter impedance.

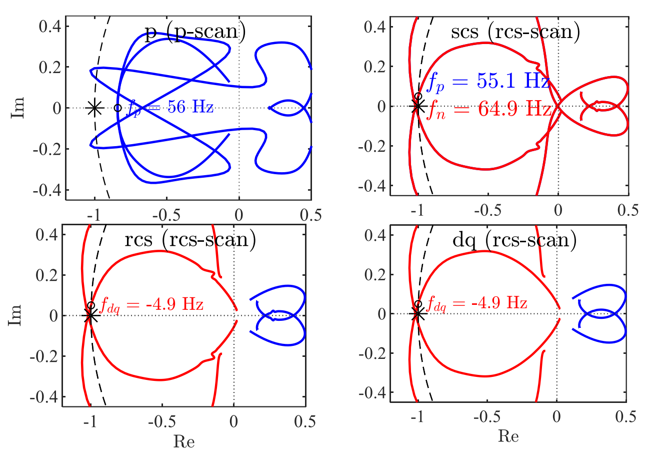

Fig. 7. Nyquist plots of the system's open-loop gain at the point of interconnection of the GFM converter.

Overall, this confirms that an impedance domain accounting for mirror-frequency coupling should be chosen for IBSA, even if asymmetric coupling seems negligible, as observed in Fig. 6. This is especially true if IBRs with asymmetric coupling are closely connected.

IV. Conclusion

This paper provides a concise summary of impedance modelling domains and their characteristics for the assessment of stability in multi-inverter-based resources systems. The differences between the models are illustrated via case studies of distinct grid components, providing an intuitive understanding of merits and drawbacks.

Based on the observations, the following guidelines for the impedance domain choice can be given: The influence of coupling on the studied frequency range needs to be determined by either 1) visually assessing the asymmetry of the off-diagonal impedance matrix elements in scs- or rcs-domain, or by 2) comparing the p-scan with the p-converted scs- or dq-scan to directly observe the discrepancy caused by coupling. If coupling is not observed, impedance-based stability analysis (IBSA) can safely be performed with p-scanning and p-impedances. Otherwise, p-scanned impedances should not be used, but p-impedances converted from dq-, rcs-, or scs-domain can be used as a support for understanding system characteristics. The authors would recommend scanning and IBSA in dq-domain, because of its simplicity and slight computational speed advantages over rcs-scanning, and convert dq- to other domains, if needed. For islanded systems, where the fundamental frequency is not known exactly, the rcs-scan can be used.

V. References

[1] N. Hatziargyriou *et al.*, "Definition and Classification of Power System Stability – Revisited & Extended," in *IEEE Transactions on Power Systems*, vol. 36, no. 4, pp. 3271-3281, July 2021.

[2] Y. Cheng et al., "Real-world subsynchronous oscillation events in power grids with high penetrations of inverter-based resources," IEEE Trans. Power Syst., vol. 38, no. 1, pp. 316–330, Jan. 2023.

[3] L. Fan, and Z. Miao, "Admittance-Based Stability Analysis: Bode Plots, Nyquist Diagrams or Eigenvalue Analysis?," in *IEEE Transactions on Power Systems*, vol. 35, no. 4, May. 2020.

[4] L. Harnefors, "Modeling of Three-Phase Dynamic Systems Using Complex Transfer Functions and Transfer Matrices," in *IEEE Transactions on Industrial Electronics*, vol. 54, no. 4, pp. 2239-2248, Aug. 2007.

[5] A. Rygg, M. Molinas, C. Zhang and X. Cai, "A Modified Sequence-Domain Impedance Definition and Its Equivalence to the dq-Domain Impedance Definition for the Stability Analysis of AC Power Electronic Systems," in IEEE Journal of Emerging and Selected Topics in Power Electronics, vol. 4, no. 4, pp. 1383-1396, Dec. 2016.

[6] L. Meng, U. Karaagac, A. Pavani, J. Mahseredjian and K. Jacobs, "Examination of EMT-Type Impedance Scanning Techniques for Small Signal Stability Assessment of Inverter Based Resources," in *IEEE Transactions on Power Delivery*, vol. 40, no. 3, pp. 1607-1620, June 2025.

[7] L. Meng, U. Karaagac, K. Jacobs, "A new sequence domain EMT-level multi-input multi-output frequency scanning method for inverter based resources," in *Electric Power Systems Research*, Volume 220, 2023, p. 109312.

[8] A. Rygg, M. Molinas, C. Zhang, and X. Cai, "Coupled and Decoupled Impedance Models Compared in Power Electronics Systems," 2016, arXiv:1610.04988. [Online]. Available: https://arxiv.org/abs/1610.04988

[9] EMTP®, Example File "GFMinverter_V2.ecf", https://www.emtp.com/

[10] X. Gao, D. Zhou, A. Anvari-Moghaddam and F. Blaabjerg, "Stability Analysis of Grid-Following and Grid-Forming Converters Based on State-Space Modelling," in *IEEE Transactions on Industry Applications*, vol. 60, no. 3, pp. 4910-4920, May-June 2024.

[11] S. Shah, P. Koralewicz, V. Gevorgian and R. Wallen, "Sequence Impedance Measurement of Utility-Scale Wind Turbines and Inverters – Reference Frame, Frequency Coupling, and MIMO/SISO Forms," in *IEEE Transactions on Energy Conversion*, vol. 37, no. 1, pp. 75-86, March 2022.

979-8-3315-8138-1